

Effect of the curved vane on the hydraulic response of the bridge pier

Rafi M. Qasim¹, Tahseen A. Jabbar¹ and Safaa H. Faisal^{*2}

¹Department of Fuel and Energy Eng., Southern Technical University, Basra, Iraq

²Department of Thermal Mechanics Eng., Southern Technical University, Basra, Iraq

(Received April 10, 2022, Revised August 30, 2022, Accepted September 13, 2022)

Abstract. Hydrodynamic field alteration around a cylindrical pier using a curved vane is numerically investigated. The curved vane with various angles ranged from 10 to 220 degree is placed at the upstream of the cylindrical pier. Laminar flow is adopted in order to perform the steady-state analysis. It is found that the flow separation leads to the formation of four bubbles depending on the value of the curved vane angle. Two bubbles are located in the region between the rear of the curved vane and the leading surface of the cylindrical pier, while the remaining two bubbles are located at the wake zone behind the cylindrical pier. Numerical analysis is performed to reveal the hydrodynamic field and influence of curved vane on the formation and evolution of the bubbles. It is found that the center and size of the bubble depend mainly on the value of the curved vane angle. It is observed that the flow velocity vector shows clearly the alteration in the flow velocity direction especially at the leading surface and rear surface of the curved vane owing to the occurrence of flow separation and flow dissipation along the circumference of the vane.

Keywords: bridge pier; CFD; circular vane; flow field; laminar flow

1. Introduction

Normally fluid obstruction around individual objects illustrates significant physical phenomena such as vortex generation and turbulence. Many practical mechanical characteristics, comprising buoyancy force and drag force, as well as pressure coefficient significantly affect the vortex generation mechanism (Bimbato *et al.* 2011). Kwon and Choi (1996) did a simulation to investigate the control of laminar vortex shedding behind a circular cylinder by utilizing a splitter plate. It is found as the splitter plate length is greater than a critical length, the vortex shedding will be disappeared completely, while the increase in the plate length especially when the plate length is close to the cylinder diameter, the vortex shedding Strouhal number is decreasing rapidly, also the splitter plate led to the important reduced in the net drag. Graf and Istiarto (2002) studied the flow fields in the planes downstream and the upstream of a cylinder and vertically in the hole of the scour. Becker *et al.* (2002) investigated experimentally the three-dimensional flow around an obstacle with different aspect ratios. The obstacle has a rectangular shape. The studies were performed using different kinds of flow visualization techniques and a laser Doppler anemometry system. Alam *et al.*

*Corresponding author, Dr., E-mail: s_hfaisal100@stu.edu.iq

(2003) experimentally studied the influences of tripping rods on the flow characteristics and the fluid forces acting on the cylinder has a circular cross-section with Reynolds number of 5.5×10^4 . Saha *et al.* (2003) performed a comparison between flow past a cylinder in three and two dimension respectively. The cylinder have square cross section, in this comparison $Re = 250$. Reichl *et al.* (2005) and Bouscasse (2017) investigated numerically the flow pass a cylinder close to the free surface. The behavior of wake at $Re = 180$, Fr range values between 0 and 0.7 with gap ratio between 0.1 and 5 is investigated. Various deformation of the free surface depends on the adopted Fr can be shown. Hsieh and Chen (2006) did a numerical study with a low Reynolds number around a cylinder placed symmetrically in a channel. Hwang and Yang (2007) studied numerically the influence of the two splitter plates of the same length, on the reduction of the drag of the circular cylinder when the length of the two plates is equal to the cylinder diameter. The first plate is placed upstream of the cylinder while the second plate is placed downstream of the cylinder near the wake zone. Rajani *et al.* (2009) dealt with the analysis of the flow passes a circular cylinder in two dimensions and three dimensions in various laminar flow regimes. Ali *et al.* (2011) did a numerical investigation to study the flow pattern over a cylinder have square section, without and with a splitter plate respectively. In this study $Re = 150$. The splitter plate length diverse from $L = 0.5D$ to $L = 6D$, where D is pointed to side length of cylinder. They obtained a strong hydrodynamic interference at cylinder wake owing to the existence of splitter plate. Finally, they classified the flow behavior into three regimes. Rajani *et al.* (2013) made a numerical study in two dimension considering laminar unsteady flow around a cylinder into a channel; the cylinder has circular cross section. The study provided the following: reduced in the wake length and shift in the flow separation. Xu *et al.* (2013) studied the hydrodynamic characteristics of the bluff cylinder experimentally, here the cylinder oscillated in the transverse direction. The adopted flow is steady and the Reynolds number equals 2×10^5 . The influence of Reynolds number, non-dimensional frequency, oscillating amplitude on phase angle, lift force, and drag force are studied. Vortex shedding mechanics is used to clarify the results of the experiment. Wu *et al.* (2014) investigated numerically the flow control around a cylinder with a circular section by using flexible filament. The filament is linked to the cylinder at the base. On the other hand, the filament leading end is considered fixed while the trailing end is considered free. Laminar flow is adopted in the analysis with a Reynolds number equal to 150. Deng *et al.* (2014) investigated experimentally the wave crossing a vertical cylinder when the water depth is considered transitional. Regular waves, irregular waves, and focused waves are adopted in the experimental investigation. This investigation dealt with the interaction between wave and cylinder. Ahmed (2015) did a numerical investigation about vortex shedding considering laminar flow with $40 \leq Re \leq 300$. Two dimensional, incompressible and unsteady flow is adopted for numerical solution of the hydraulic problem. Meanwhile, the results implied that the flow is unsymmetrical and unsteady when Reynolds number greater than 60, also a good comparison is obtained between the results and the previous available experiments. Zhang *et al.* (2014) performed a numerical simulation in two dimensions by utilizing unsteady Reynolds-Averaged Navier Stokes (URANS) equations and the standard $k - \epsilon$ turbulence model in subcritical and supercritical flow. Here, the adopted Reynolds number are 1×10^5 , 5×10^5 , and 1×10^6 . Ramli *et al.* (2019) dealt with the passive flow control method to suppress the vortex shedding from a cylinder that has a circular section. Perforated shrouds are employed to dominate the vortex shedding of the cylinder when the $Re = 200$. Uniform and non-uniform shrouds are employed with porosity equal to 67%. The numerical analysis is conducted by utilizing ANSYS Fluent with adopting a laminar model. Osrin *et al.* (2019) studied experimentally the flow cross a shrouded cylinder by adopting a uniform and non-uniform hole shrouds. The experiments are made to find the influence of uniform and non-

uniform holes of the perforated shrouds on the lift coefficient and the drag coefficient of the cylinder. The experiment is done in a wind tunnel and the Reynolds number is equal to 9.345×10^3 . Zhu and Zhou (2019) investigated numerically the impact of two symmetrically fins on the flow field and hydrodynamic forces of a cylinder with a circular section, where Reynolds number from 60 to 180. It is found that the separation of the boundary layer is influenced by fin strips, altering the distribution of the pressure and leading to form a recirculation zone behind the fin strips. Abdulhussein *et al.* (2019) did an experimental study to reveal how to reduce the depth of the scour, which happens around a bridge pier by using a special device. The device is placed upstream of the pier. The results show a good reduction in the depth of the scour as compared with scour around pier without using a special device. Wang *et al.* (2020) studied numerically the flow around oblique cylinder with circular section. The unsteady Reynolds Averaged Navier-Stokes equation is used to explore three dimensions external and axial flow respectively. The flow field investigation comprises coefficients of the aerodynamic force, wake flow velocities, correlations between wake flow and aerodynamic force, three-dimensional vortex structures, and axial flow respectively. Sharma and Barman (2020) investigated numerically at low Reynolds number the flow across a slotted circular cylinder. Reynolds number of the regime has ranged from 10 to 50. From the observation, it is found that the flow separation led to the formation of the bubble at Reynolds number greater than 7, also leading to the shedding at Reynolds number greater than 47 for the slotted cylinder. The slotted cylinder has three different configurations of the slot. The numerical analysis is achieved to reveal the flow pattern and the influence of the slotted cylinder on the drag coefficient, flow separation, and bubble formation at a low Reynolds number. Bordbar *et al.* (2021) performed a numerical model to investigate the local scour around single vertical piers with various cross-sectional shapes. The model solves both the sediment transport process and flow field by utilizing a coupled approach. The suggested model is tested against empirical data from the literature dealing with local scour around single vertical piers with square, circular, and diamond cross-sectional shapes. Qasim and Jabbar (2021) studied the flow pattern which is surrounded the cylinder neighboring by the vane numerically. The turbulent model is described by Reynolds Average Navier Stokes. The investigation of the hydrodynamic field includes eddy viscosity, turbulent dissipation rate, turbulent kinetic energy, turbulent intensity, flow velocity, pressure coefficient, and static pressure.

The purpose of the current study concentrated on the laminar and steady flow past a cylindrical pier nearby a curved vane located upstream of the cylindrical pier. The goals of the current numerical study can be summarized as below:

- 1- Understand the formation of the bubbles at the upstream and downstream of the cylindrical pier due to the existence of the curved vane using several values of the curved vane angle.
- 2- Understand the flow velocity vector, which reflects the occurrence of flow separation and dissipation along a circumference of the curved vane.
- 3- Investigate the direct relationship between downstream bubbles length and the value of the curved vane angle for various values of Reynolds number.
- 4- Investigate the relationship between downstream bubbles length and curved vane length considering Reynolds number.
- 5- Explore the flow velocity behavior along a radial line, which will be responsible for the formation of the bubble in the zone between the downstream of the curved vane and the upstream of the cylindrical pier.
- 6- Explore the behavior of the flow velocity in the lateral direction and longitudinal direction measured from the center of the cylindrical pier.

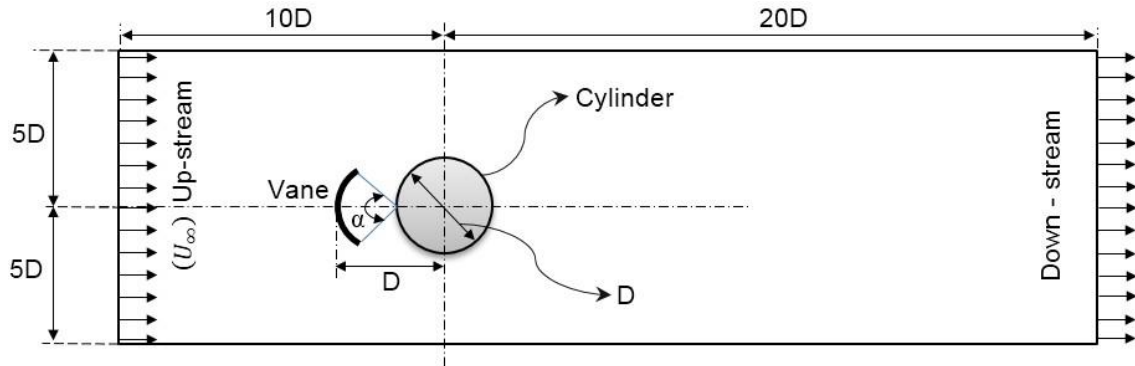


Fig. 1 The hydraulic domain setup

2. Computational domain formulation

The rectangular domain sketch given in Fig. 1 presents two dimensional steady, incompressible flow. The two-dimensional flow domain contains two different solid structures. The first one is a circular curved vane with an angle ranging from 10 degree to 230 degree with gradually incremental equal to 10 degree. The second one is the circular cylindrical pier. The circular curved vane is placed at the upstream (leading) of the circular cylindrical pier. The degree of the proximity between the curved vane and the cylindrical pier depends on the vane angle and the vane curvature. The horizontal distance between the vane leading edge and the circular cylindrical pier center is equal to the pier diameter. The curved vane center is located at the circumference of the cylindrical pier and is located directly on the stagnation point. Low Reynolds number is adopted in the computational analysis of the flow interaction - curved vane - flow - cylindrical pier (fluid-structure - interaction). The total width of the rectangular domain is taken $10D$ and the total length of the rectangular domain is taken $30D$. The distance between the center of the pier and the sides of the domain is equal to the $5D$, while the distance between the inlet and the center of the pier is equal to the $10D$ and the distance between the outlet and the center of the pier is equal to the $20D$. The no-slip boundary conditions are imposed on the circular curved vane, cylindrical pier, and channel sides (walls). In addition, the entering flow velocity boundary condition is applied at the inlet ($= U_\infty$) and zero-gauge pressure is applied at the outlet. Water is used as a fluid flow along the two-dimensional domain with constant physical properties.

3. Numerical setup and mesh independent

The CFD governing equations that will be used for the simulation are the conservation of momentum equations and incompressible fluid continuity equation given as (Qasim and Jabbar 2021)

$$u \frac{\partial u}{\partial x} + v \frac{\partial u}{\partial y} + w \frac{\partial u}{\partial z} = -\frac{1}{\rho} \frac{\partial P}{\partial x} + \frac{\mu}{\rho} \left(\frac{\partial^2 u}{\partial x^2} + \frac{\partial^2 u}{\partial y^2} + \frac{\partial^2 u}{\partial z^2} \right) \quad (1)$$

$$\frac{\partial v}{\partial x} + v \frac{\partial v}{\partial y} + w \frac{\partial v}{\partial z} = -\frac{1}{\rho} \frac{\partial P}{\partial y} + \frac{\mu}{\rho} \left(\frac{\partial^2 v}{\partial x^2} + \frac{\partial^2 v}{\partial y^2} + \frac{\partial^2 v}{\partial z^2} \right) \quad (2)$$

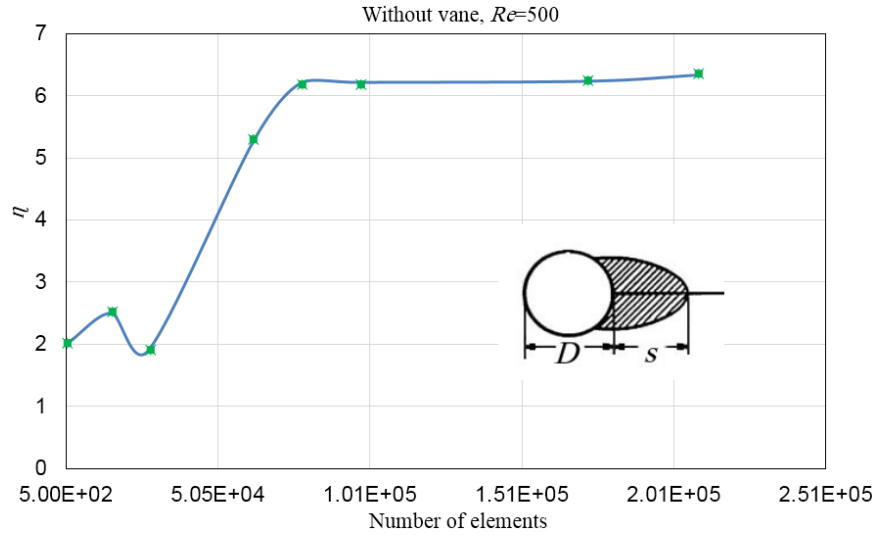


Fig. 2 Mesh independent

$$u \frac{\partial w}{\partial x} + v \frac{\partial w}{\partial y} + w \frac{\partial w}{\partial z} = -\frac{1}{\rho} \frac{\partial P}{\partial z} + \frac{\mu}{\rho} \left(\frac{\partial^2 w}{\partial x^2} + \frac{\partial^2 w}{\partial y^2} + \frac{\partial^2 w}{\partial z^2} \right) \quad (3)$$

$$\frac{\partial(\rho u)}{\partial x} + \frac{\partial(\rho v)}{\partial y} + \frac{\partial(\rho w)}{\partial z} = 0 \quad (4)$$

Elements number that are adopted in the analysis have a major impact on the flow characteristics especially the flow velocity of the water. Fig. 2 illustrates the variation of the ratio between bubble length s to the cylinder diameter D . This ratio is defined as (Sharma and Barman 2020)

$$\eta = \frac{s}{D} \quad (5)$$

It is normal during the process of changing the number of elements to find the optimal number that saves execution time and does not affect the results, to see the ratio η fluctuate, whether up or down until we see stability regardless of the number of elements. It is clear that the value η is constant when the number of the elements is greater than 7.7×10^4 .

4. Validation

Before investigating the effect of the curved circular vane on the cylindrical pier, some previous tests have been performed to assess the validity of the numerical procedure. The proposed case to make the validation is that one suggested by Rajani *et al.* (2009). The case refers to the two-dimensional flow analysis around cylinder. Fig. 3 gives a summary between the present prediction and the results found in the previous study; the comparison gives a good agreement. The validation is done for two dimensional analysis of flow with Re range from 25 to 300 with respect to the present paper but from 0 to 300 in the paper of Rajani *et al.* (2009), a reasonable convergence in the values of separation angle over the range of Re is found. For both studies there is no contrast in the obtain results.

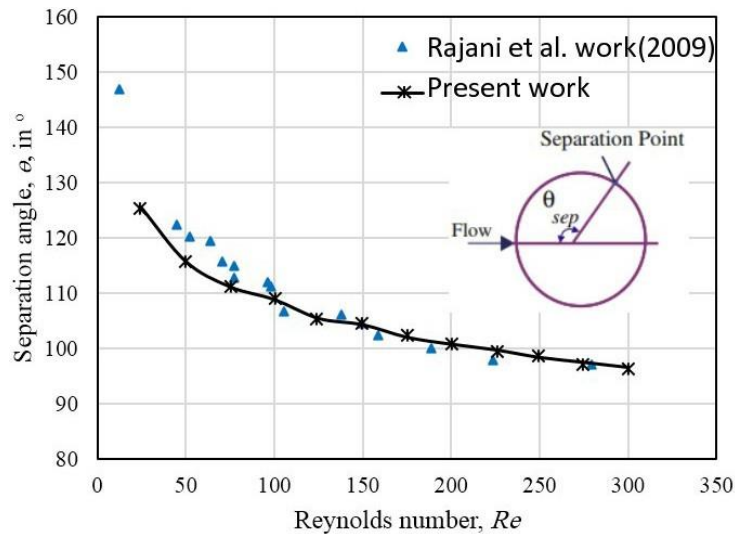


Fig. 3 Relationship between separation angles and Reynolds number

5. Results and discussion

The main pivotal aspect of the circular curved vane is reducing the stagnation pressure on the leading of the cylindrical pier by mean of the transfer the position of the stagnation point (location of the maximum pressure) from the front face of the pier or leading of the pier to the front face of the curved vane. Here, the location of minimum pressure and rising pressure will change relying on the curved vane angle. The pressure is produced and developed at the front face of the curved vane. The flow undergoes from two different processes when encountering the curved vane. These processes are flow separation and flow dissipation.

Fig. 4 shows both the flow streamlines and velocity vectors for the hydrodynamic field surrounding the curved vane and the cylindrical pier for various curved vane angles. It is evident from the figure that the bubbles will be formed and evolution in the region between the curved vane downstream and in front of the cylindrical pier (wake zone between downstream of the vane and upstream of the cylindrical pier). These bubbles develop and vanish completely. Also, the size and the position of these bubbles rely on curved vane angles and Reynolds numbers. The response of the bubbles essentially depends on the interference among the hydraulic mechanism stabilities of the vane and the cylinder respectively. It is observed from the figure that one bubble exists and can be described as quite small, this happens when the curved vane angle is equal to 20 degree. When the curved vane angle ranges from 30 degree to 100 degree two bubbles form in the zone between the rear of the curved vane and the leading surface of the cylindrical pier. The two bubbles begin to move toward the sides of the cylindrical pier along the cylinder circumference. This happens when the curved vane angle values range between 100 degree and 200 degree. After 200 degree till 230 degree, the bubbles will vanish completely. This dramatic hydraulic behavior is attributed to the following reasons; mobile separation points along the circumference of the cylindrical pier and the curved vane, these points can be considered as a common feature for both the vane and the cylinder. When the curved vane angle increases the circumference of the vane will be increased directly, therefore the curved vane edges (or ends) become close to the sides of the cylindrical pier. Here, the

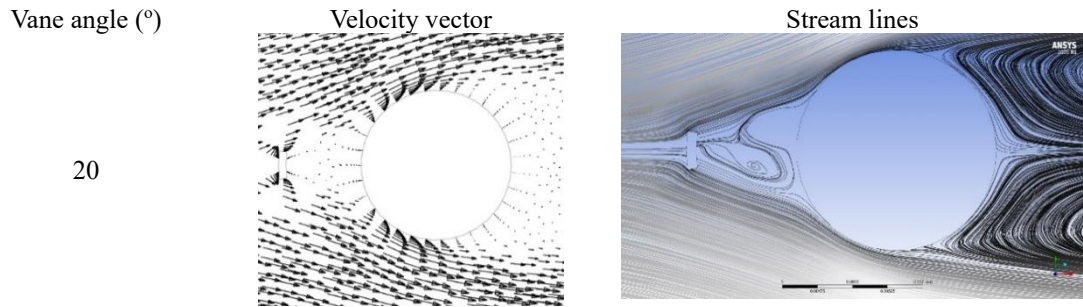
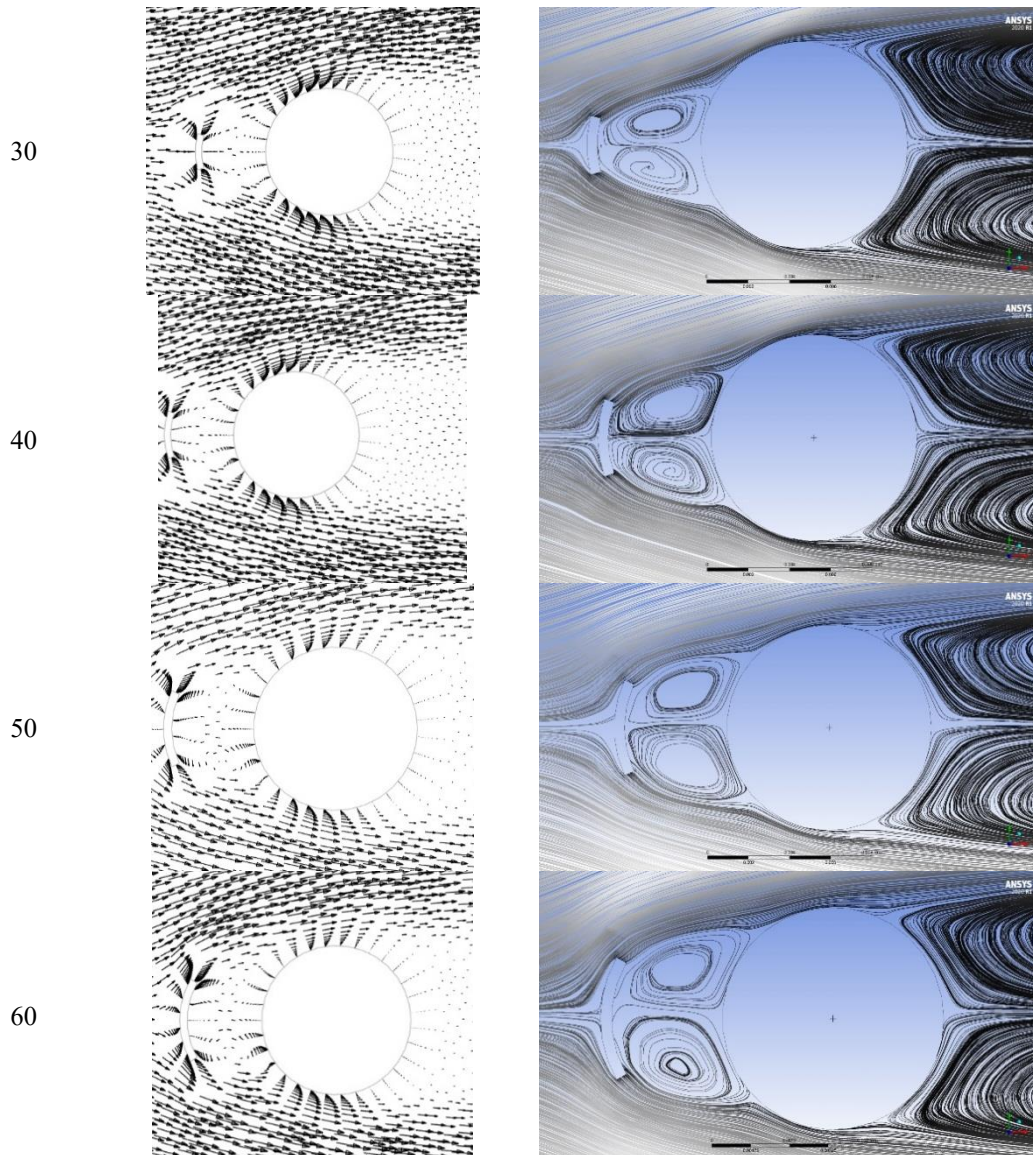


Fig. 4 Streamlines and velocity vector for the region between the curved vane and cylindrical pier ($Re = 500$)



70

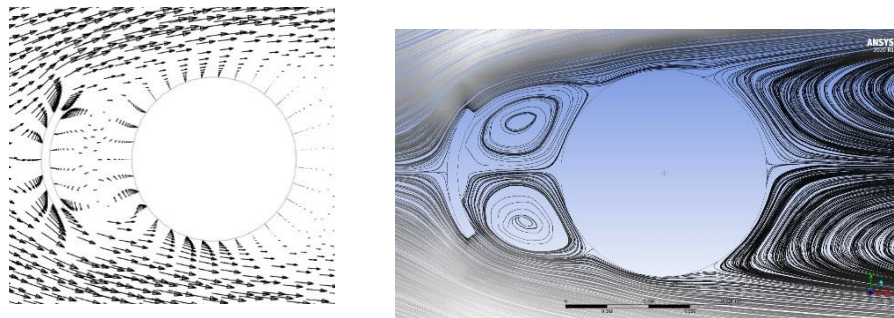


Fig. 4 Continued

locations of the water flow separation points become nearest and interfere with each other. This interference led to shortages in the potent of the bubbles and as a result, the bubbles become vanish. Clearly, this happens when the angle of the curved vane is between 200 degree and 230 degree as shown in Fig. 4. In addition, the curved vane reduces the stagnation pressure at the upstream of the cylindrical pier by friction. This means that the stagnation point will be shifted from the upstream of the cylindrical pier to the upstream of the curved vane. This shifting leads to reduce the pressure at the leading surface of the cylindrical pier, so this process will dominate the formation of the bubbles in the region between the cylinder and the curved vane. Also, the existence of the curved vane causes an excessively large deficit in the flow momentum and this led to the alteration in the flow velocity at the upstream of the cylindrical pier. This will be reflected directly in the bubble's formation and position. Fig. 4 shows the flow velocity vector at the curved vane leading, curved vane rear and upstream of the cylindrical pier (velocity vector of the flow field surrounding the vane and the cylinder) for different curved vane angles. It is observed that the velocity vector is symmetrically regardless of the value of the curved vane angle but the intensity of the flow vector varies with the curved vane angle. For the case when the curved vane angle is ranged between 20 to 70 degree, the flow velocity can be considered smooth while when the curved vane angle is ranged between 80 to 220 degree, the flow velocity can be considered higher as compared with the previous velocity. Also, the same figure illustrates that the velocity vector in the region between the rear of the curved vane and the leading surface of the cylindrical pier is disappeared approximately when the vane angle is equal to 200 degree and the velocity vanishes completely for the vane angle 210 and 220 degree respectively.

As the velocity become vanishes, this will give confirmation about the absence of the bubbles in the region between the rear of the curved vane and the leading surface of the cylindrical pier. The separation in the flow is clearly shown from the change in the direction of the velocity vector. In fact, the curved vane length (or angle) supported by the shortages in flow momentum at the leading surface of the curved vane can be considered the prevalent variables in controlling the bubbles formation. Moreover, Fig. 4 shows the streamline for various values of curved vane angle. The figure gives the contrast in streamline contour. Here, this contrast in flow deformation happens owing to the variation in the volumetric flow and flow velocity. Actually, the principle of the curved vane operation rely on deflect the direction of the flow, separate the flow, and dissipate the flow. All these processes lead to change in the flow velocity magnitude and volumetric flow and share in produce nonsymmetrical streamline. In addition, the vane circumference has a vital role in control the shape of the streamline.

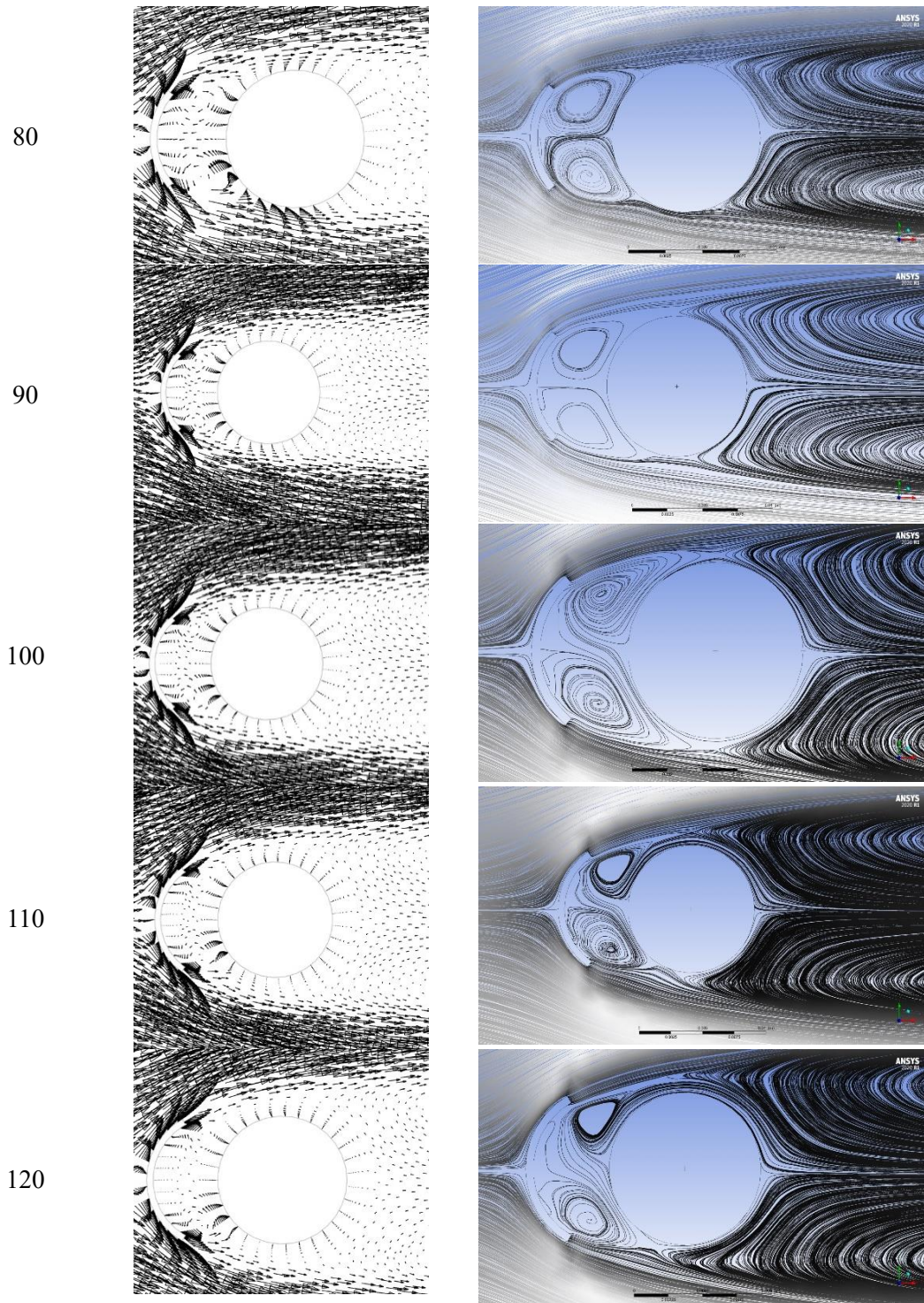


Fig. 4 Continued

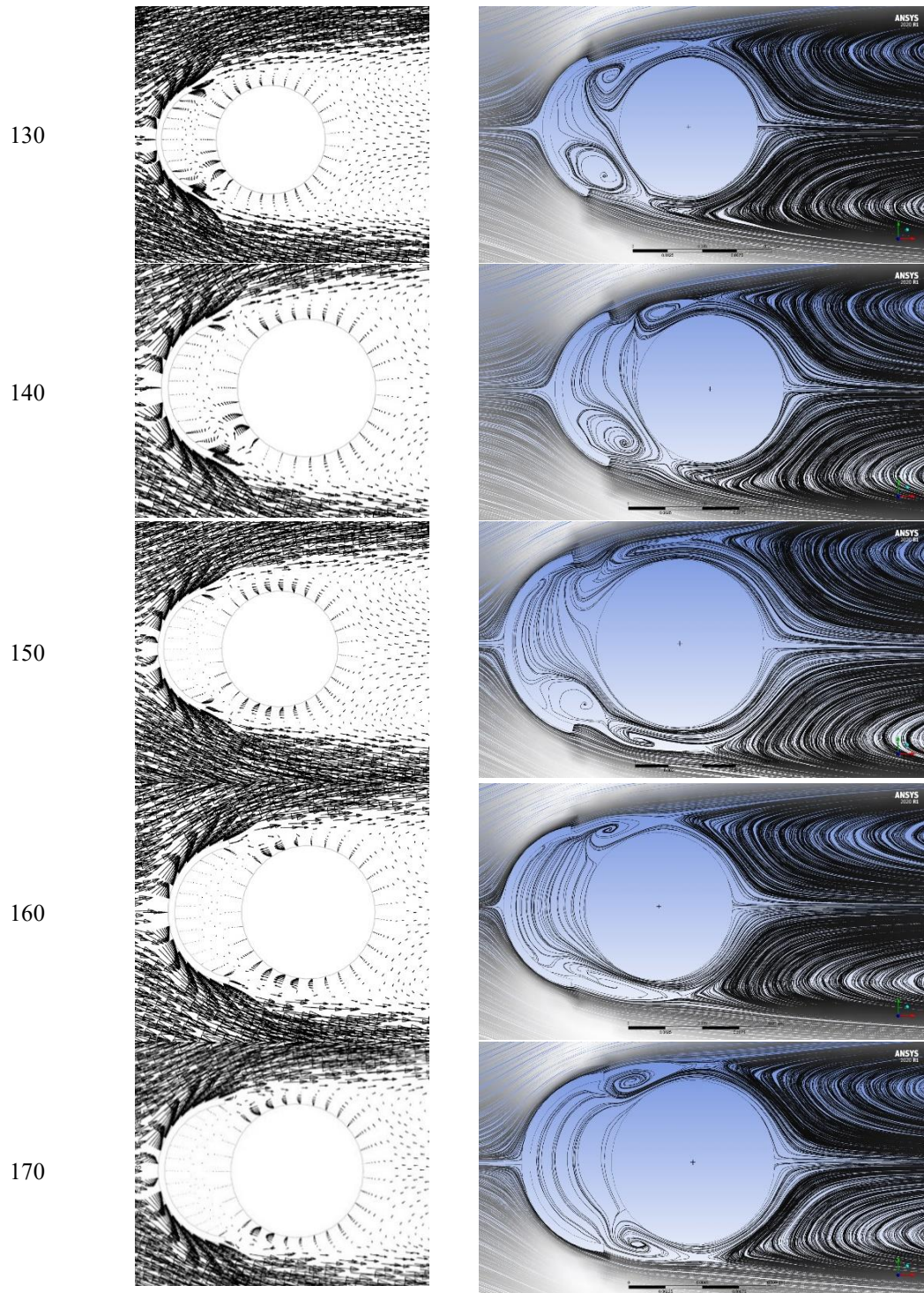


Fig. 4 Continued

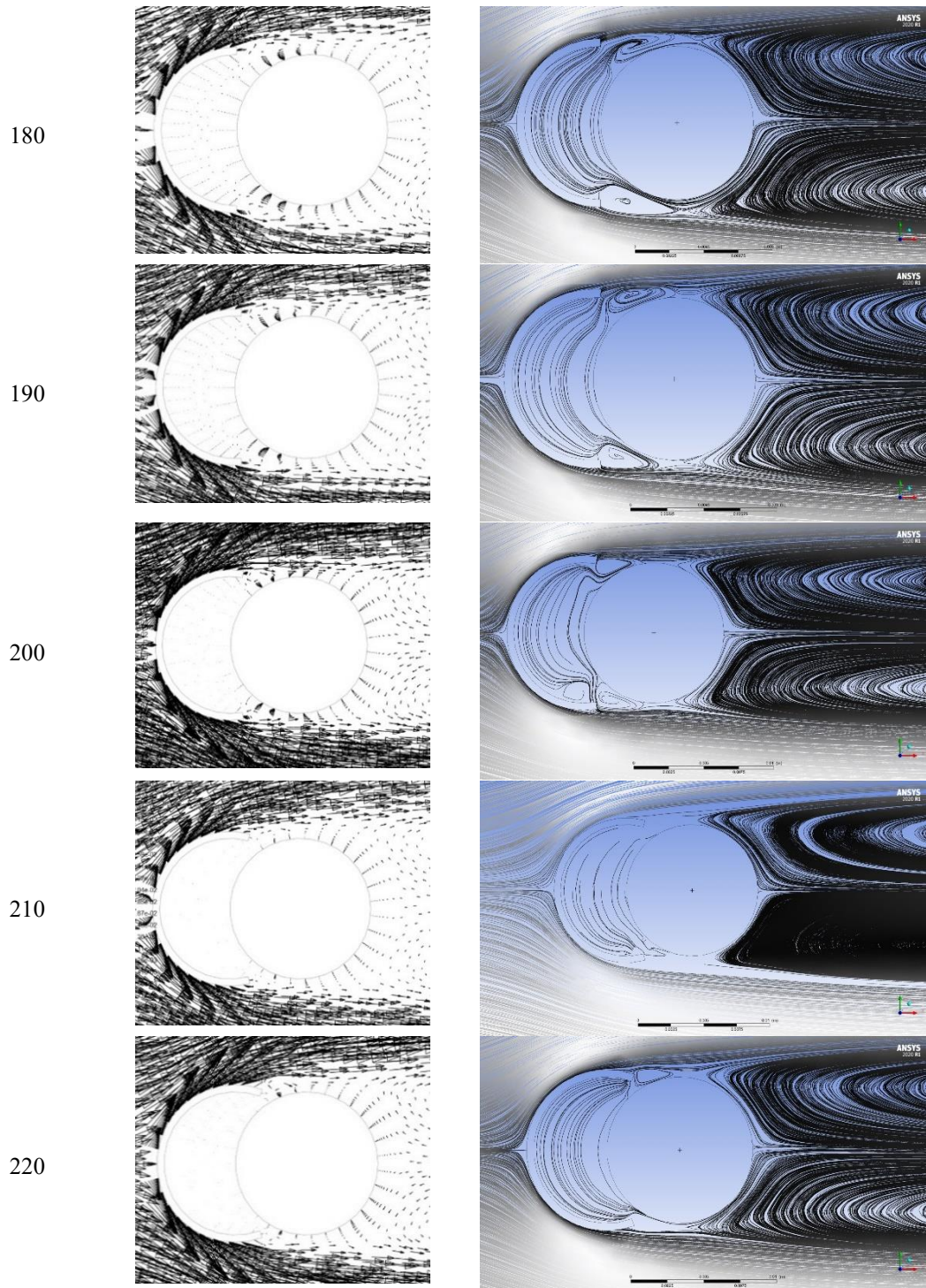


Fig. 4 Continued

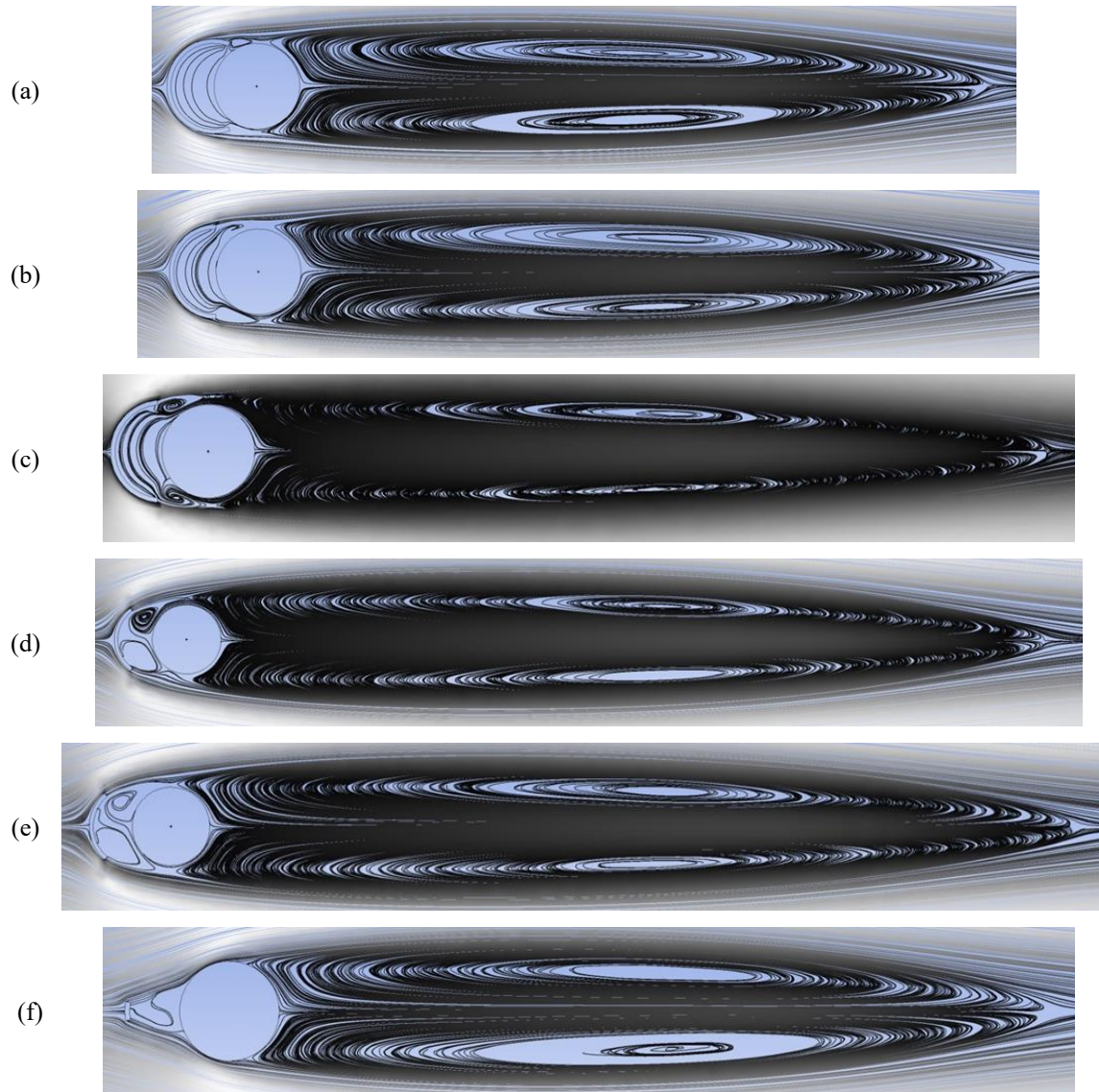


Fig. 5 The bubbles formation at the downstream of the cylindrical pier ($Re = 500$), (a) $\alpha = 220^\circ$, (b) $\alpha = 180^\circ$, (c) $\alpha = 170^\circ$, (d) $\alpha = 110^\circ$, (e) $\alpha = 100^\circ$, and (f) $\alpha = 20^\circ$

Now we deal with the bubble's formation at the downstream of the cylindrical pier (wake region). Fig. 5 shows the streamline contour for some chosen angles of the curved vane. Generally, the bubbles have an ellipse shape with a center far from the cylindrical pier center, but the length and width of the bubbles depend on the curved vane angle and Reynolds number. When the curved vane angle ranges from 180 to 220 degree, the downstream bubbles comprise more intensive streamlines, while when the angle range from 110 to 170 degree, the bubbles become less intensive in streamlines as compared with previous bubbles and the bubbles become moderately dense in the streamlines when the angle range is from 20 to 100 degree.

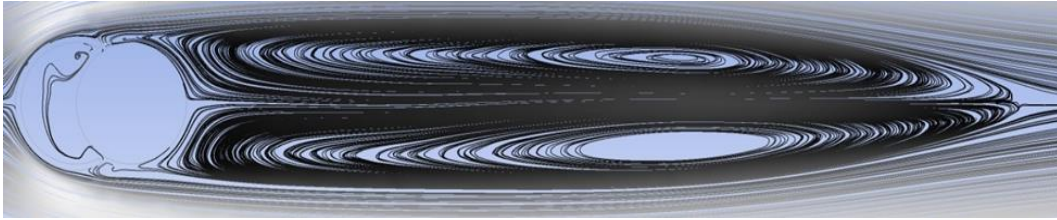


Fig. 6 The bubbles formation downstream of the cylindrical pier without curved vane ($Re = 500$)

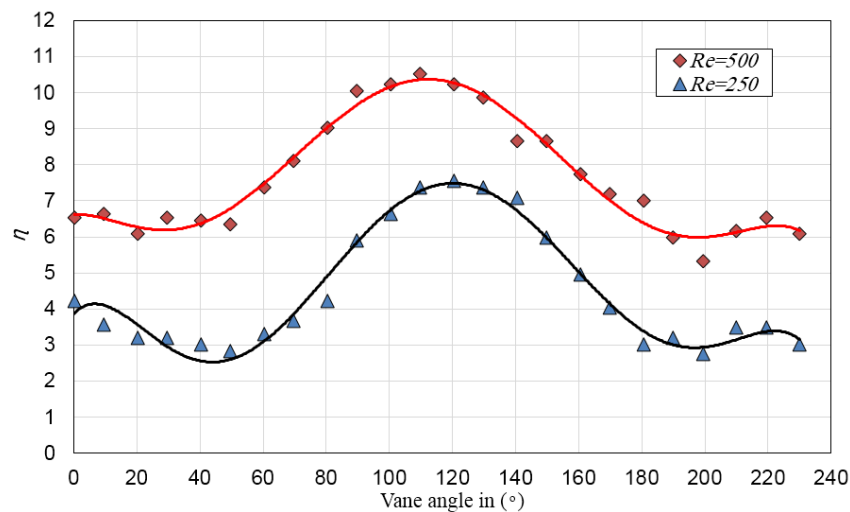


Fig. 7 Variation of η with curved vane angles for two Re numbers

Fig. 6 shows the bubbles formation at the downstream of the cylindrical pier without curved vane; it is obvious the bubbles have ellipse shape with center so far from the cylindrical pier center as compared with the bubble's formation with the existence of the curved vane. The streamline indicates the flow deformation, i.e., when the curved vane angle increases the flow deformation will increase. The competitive behavior between the two bubbles relies on the curved vane angle values.

A very motivating analysis can be performed to assess the relationship between the vane curved angle values and the ratio of the bubble length s to the cylinder diameter D . The bubble length is measured from the cylinder pier downstream stagnation point to the reattachment point. Fig. 7 illustrates the relation between ratio η and the values of the curved vane angles for different Reynolds numbers. The investigation adopted two different values for Reynolds number these values are 500 and 250. It is noticed a nonlinear trend between the ratio η and the curved vane angle values for the two values of Reynolds number. It is visible from the figure that the curve, which has Re equal to 500, lay over the curve, which has Re , equals 250 regardless of the angle value. The figure obviously illustrates a considerable increase in the ratio η for the angle range from 30 to 110 degree when Re equals 500 and for the angle range from 50 to 120 degree when Re equals 250. In addition, the figure clearly illustrates a considerable decrease in the ratio η for the angle range from 110 to 200 degree when Re is equal to 500 and for the angle range from 10 to 40 degree when Re equals 250. In addition, the figure obviously shows a considerable decrease in η for the angle range

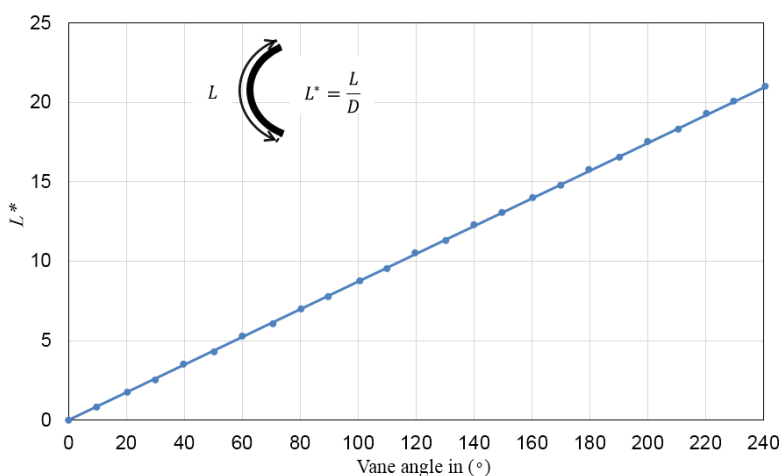


Fig. 8 Relationship between the ratio L^* and the curved vane angle

120 to 200 degree when Re equals 250. Generally, the two curves show approximately harmonic trend. For Reynolds number equal to 500, the length of the longest bubble happens when the ratio η equal to 10.7 and the curved vane angle equal to 110, while the length of the shortest bubble happens when the ratio η equal to 5.5 and the curved vane angle equal to 200. for Reynolds number equal to 250, the length of the longest bubble happens when the ratio equal to 7.8 and the curved vane angle equal to 120, while the length of the shortest bubble happens when the ratio equal to 2.7 and the curved vane angle equal to 40. A very significant estimation can be found from the figure, the length of the downstream bubbles when the cylindrical pier without curved vane (angle=0). Here the ratio η equal to 6.6 when Reynolds number equal 500, this means the length of the bubble greatest than the shortest bubble when Reynolds equal 500. But when the ratio η equal to 4 when Reynolds number equal 250, this means the length of the bubble greatest than the shortest bubble when Reynolds equal 250. With careful monitoring, it can be inferred that the length of the bubble for normal cylindrical pier is slightly greater the shortest length of the bubble with curved vane. The results obtained from Fig. 7 strengthen the obtained results in Figs. 5 and 6. Furthermore, the longest and shortest length of the bubbles expresses the level of the streamlines deformation, which incurred during the existence of the curved vane as compared without vane.

Fig. 8 shows the relationship between the ratio L^* and the curved vane angle. Here, L^* represent the ratio between the curved vane length (circumference), L and the cylindrical pier diameter, D , i.e.

$$L^* = \frac{L}{D} \quad (6)$$

It is evident from the figure that there is a direct proportional relationship between the ratio L^* and the curved vane angle based on the fact as the angle value increases, then the length of the curved should be increased directly. Fig. 8 leads to strengthening the results obtained in Fig. 4. For more clarification, when the curved vane length increased then the number of the mobile separation points will be increased and this will lead to the alteration in the flow velocity. In addition, the increase in the curved vane length led to increasing in the friction between the flow and the circumference of the vane (increase the dissipation of the flow velocity).

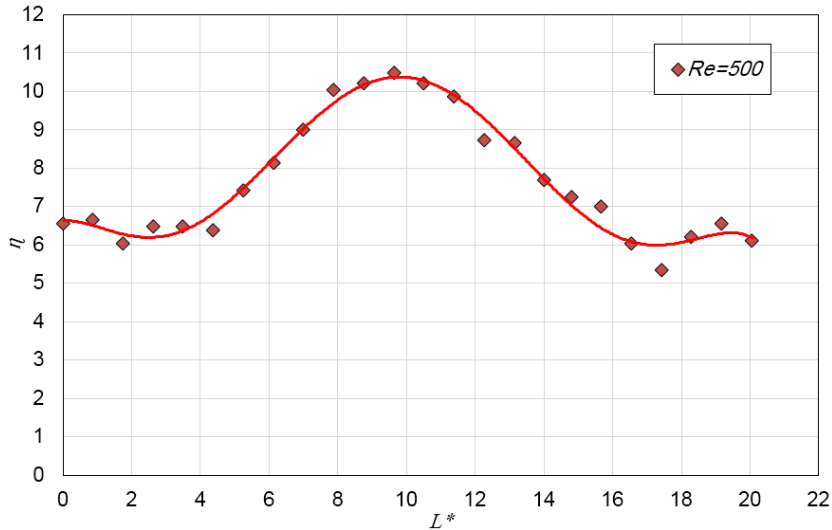


Fig. 9 Relationship between the ratio η and the ratio L^*

Fig. 9 shows the alteration in the relation between the ratio L^* and the ratio η for Reynolds number value equal to 500. It is apparent the figure can be considered symmetrical about the ratio L^* equal to approximately 10 and this give a good indicator with Fig. 7. The relationship between the ratio L^* and the ratio η starts with an increase gradually until it reaches the peak value and then it decreases gradually. Actually, Fig. 9 explains a very significant agreement point, which is the length of the curved vane (circumference) will control the elongation of the downstream bubbles and contribute to the inlocated of the bubble center.

Meanwhile, it is not necessarily that the increase in curved vane length will lead to an increase in the downstream bubble’s length. Therefore, we can infer that the location of the mobile separation points along the vane circumference will control the length of the downstream bubbles regardless of the vane length. A significant observation can be obtained which is the trend in the relationship of the Fig. 9 is identical with the trend in the relationship drawn in Fig. 7 for Reynolds number equal to 500.

Figs.10(a)- 10(c) illustrate the variation between the ratios r^* and U^* with different curved vane angles. The ratios r^* and U^* are defined by

$$r^* = \frac{r}{D} \tag{7}$$

$$U^* = \frac{u}{U_\infty} \tag{8}$$

Where r is the radial distance starting from the stagnation point at the upstream of the cylindrical pier and crossing the curved vane.

u : is the flow velocity magnitude in the x -direction along the radial distance.

U_∞ : is the flow velocity that is entering the hydraulic domain (inlet flow velocity).

The figures show a very noticeable and interesting nonlinear relationship between the two ratios based on the value of the curved vane angle. Fig. 10(a) is plotted for curved vane angle range from 10 to 80 degree. The figure clarifies that when the radial distance value is between the stagnation

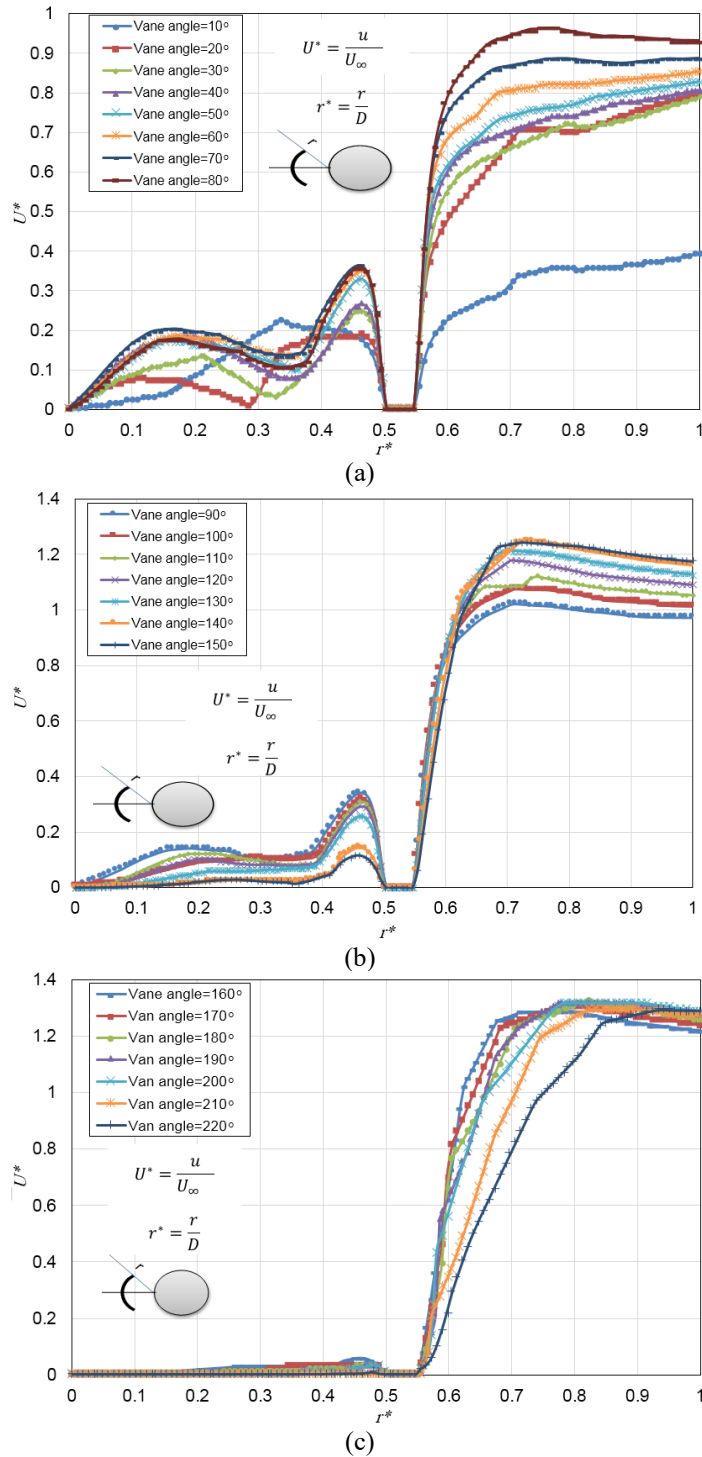
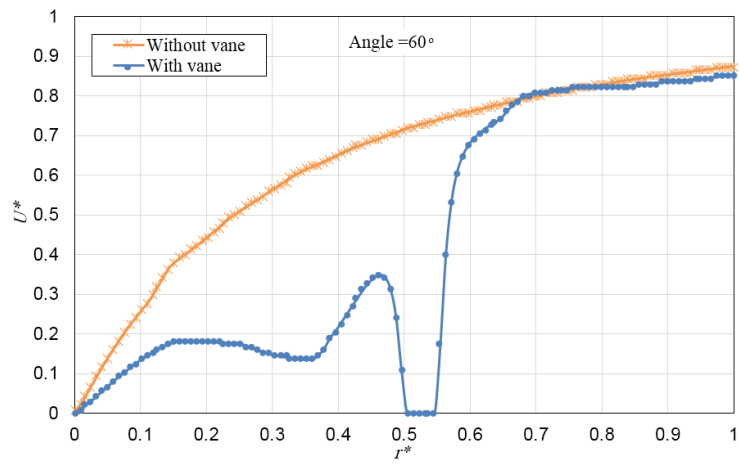
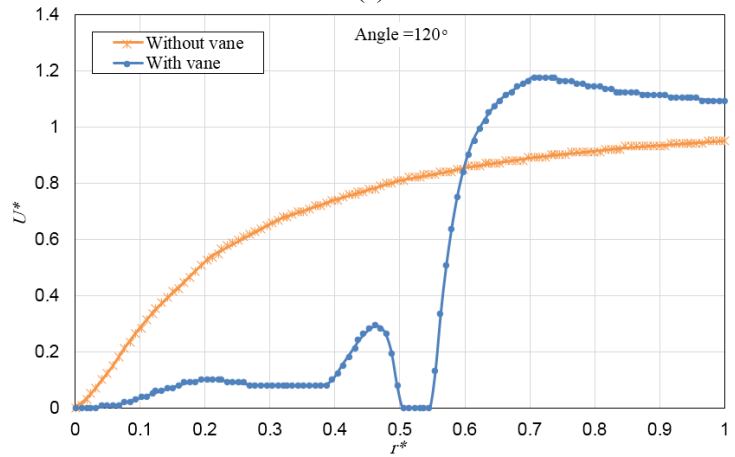


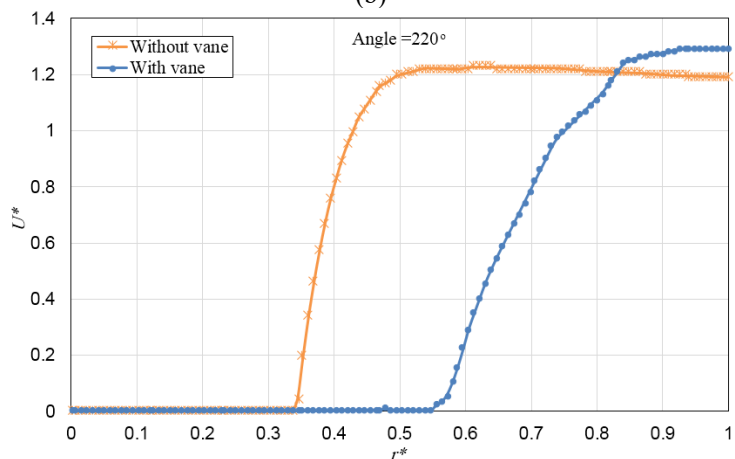
Fig. 10 (a) Variation of the ratio U^* with the ratio r^* for different vane angles $10^\circ - 80^\circ$, (b) Variation of the ratio U^* with the ratio r^* for different vane angles $90^\circ - 150^\circ$ and (c) Variation of the ratio U^* with the ratio r^* for different vane angles $160^\circ - 220^\circ$



(a)



(b)



(c)

Fig. 11(a). The variation of U^* with r^* for vane angle 60° , (b) The variation of U^* with r^* for vane angle 120° and (c) The variation of U^* with r^* for vane angle 220°

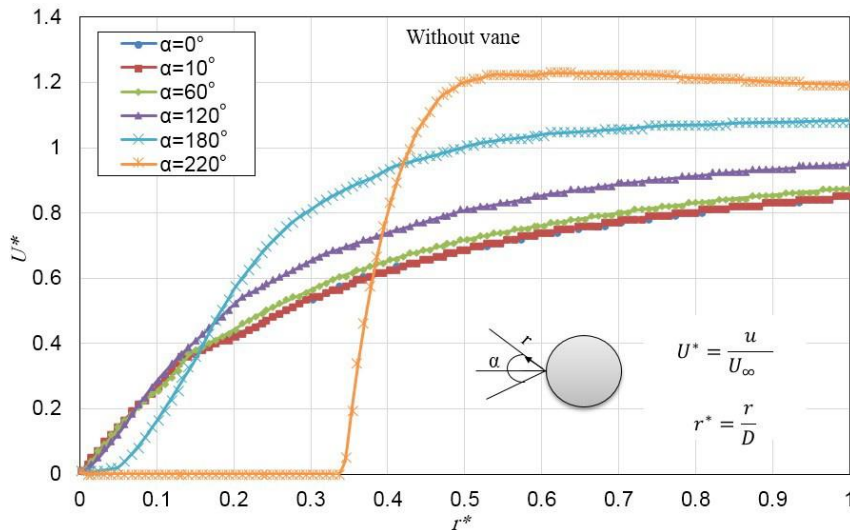


Fig. 12 Variation of the ratio U^* with the ratio r^* without curved vane

point and the circumference of the curved vane, then the flow velocity is less than the inlet flow velocity (r^* is less than 0.5). Note that at the curved vane, the flow velocity equals to zero because of the assumption that state no-slip boundary condition (r^* between 0.5 and 0.6). After the curved vane, the flow velocity is greater than the flow velocity in the region between the curved vane and the cylindrical pier until it reaches the inlet flow velocity (r^* greater than 0.6). The same conclusion is applicable for Figs. 10(b) and 10(c) taking into consideration the following.

Fig. 10(b) is plotted for curved vane angles ranging from 90 to 150 degree and Fig. 10(c) is plotted for curved vane angles ranging from 160 to 220 degree. Actually, Fig. 10 promotes the results obtained in Fig. 4, especially the flow velocity vector.

A comparison study is made to find the impact of the curved vane existence on the hydrodynamic field as compared with the case of no vane. Figs. 11(a)-11(c) deal with this comparison considering three different angles, the flow is laminar, and the Reynolds number is equal to 500. The comparison is performed in terms of the ratio r^* and the ratio U^* with the curved vane angle. Considering Fig. 11a, when the ratio r^* ranges from 0 to 0.77, then the ratio U^* for the case without a curved vane is greater than the ratio U^* with a curved vane. After the ratio r^* equals 0.78, both cases have a similar trend. Concerning Fig. 11(b), when the ratio r^* ranges from 0 to 0.6, then the ratio U^* for the case without a curved vane is greater than the ratio U^* with a curved vane. Beyond the value of the ratio r^* that is equal to 0.6, the flow velocity for the case of the curved vane is greater than the flow velocity without the existence of the curved vane. Finally, Fig. 11(c) shows that when the ratio r^* is ranged from 0 to 0.34, then both cases have a similar trend, while when the ratio r^* is between 0.34 and 0.84 then the ratio U^* for the case without curved vane is greater than the ratio U^* with curved vane. Beyond the value of the ratio r^* that is equal to 0.84, the ratio U^* for the case with curved vane is greater than the ratio U^* without curved vane. The variation in both cases is attributed to the influence of the flow velocity value and its position. For the case of existing the curved vane at the upstream of the cylindrical pier, the flow velocity undergoes to the length of the curved vane. This length dominates the mobile separation points and the flow energy dissipation by the friction. Also, it is very important to mention that the length depends mainly on the angle of the curved vane.

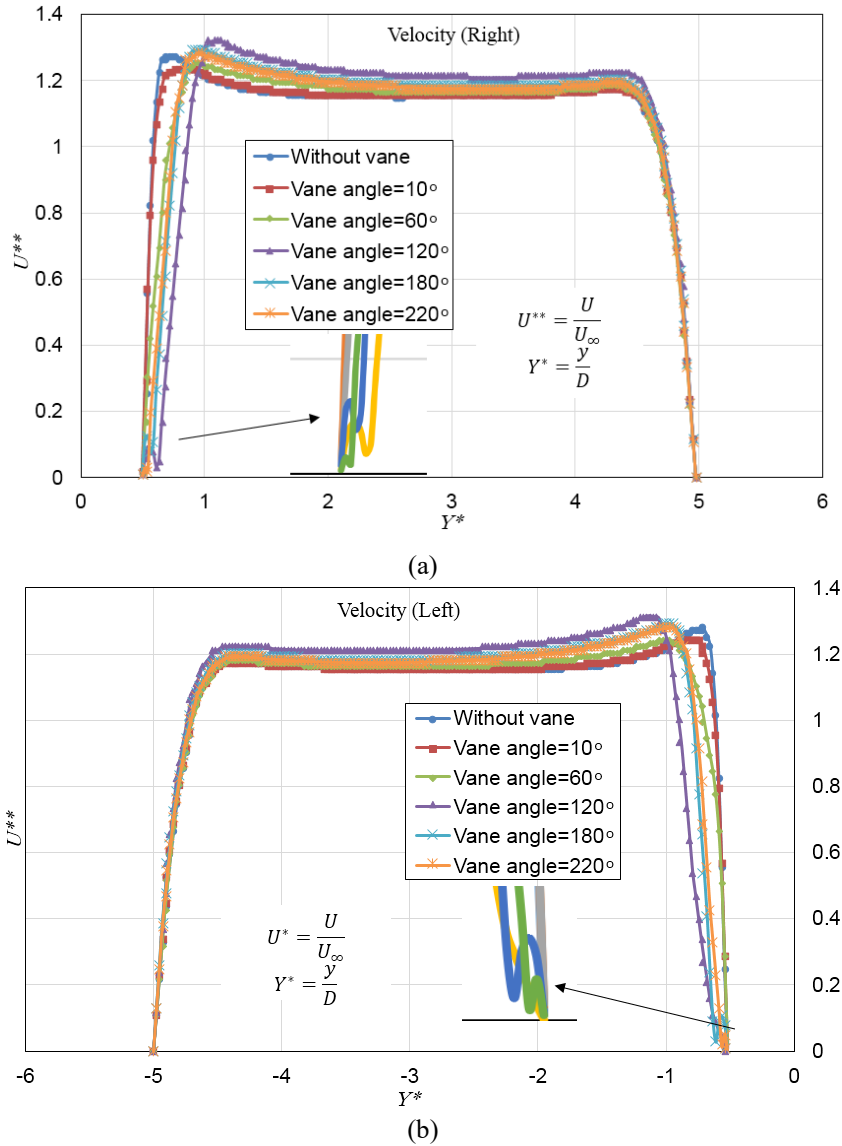


Fig. 13 (a) Variation of the ratio U^{**} with the ratio Y^* (right side) and (b) Variation of the ratio U^{**} with the ratio Y^* (right side)

Fig. 12 illustrates the variation of the ratio r^* with the ratio U^* without curved vane. This figure is drawn to explore the variation of the flow velocity along a radial line without a vane. The green curve in Fig. 12 is analogous to the orange curve in Fig. 11(c). Both of these curves are drawn without vane in order to show the velocity change relative to the distance. The figure shows that the flow velocity without the curved vane is always less than the flow velocity with the curved vane. The presence of the curved vane led to reducing the width of the flow domain and this will be reflected in the flow velocity according to the continuity equation.

Figs. 13(a) and 13(b) deals with the alteration between the ratio Y^* and the ratio U^* in the

lateral dimension of the hydrodynamic domains where the cylindrical pier center is the origin point. These two ratios are defined by

$$U^{**} = \frac{U}{U_{\infty}} \quad (9)$$

$$Y^* = \frac{y}{D} \quad (10)$$

Where U is the flow velocity magnitude, which consists of two components. These components are the lateral flow velocity (in the y-axis direction) and the longitudinal flow velocity (in the x-axis direction).

y : is the lateral distance measured from the cylindrical pier center toward the boundary of the hydrodynamic domain.

The figure is sketched to reveal the mutation that happens in the flow pattern between the two different cases, which are with and without the curved vane. It is obvious from the Figs.13(a) and 13(b) that the ratio U^{**} at or near the surface of the cylindrical pier is equal to zero because of the no-slip boundary condition. The ratio U^{**} increases gradually until the ratio Y^* approximately becomes 4.5 or -4.5. This happens because of the growth and evolution in the flow velocity in the region confined between the side surface of the cylindrical pier and the edge of the boundary. After that, the ratio U^{**} decreases gradually until it reaches zero due to the no-slip boundary condition at the edges of the domain. Based on the figure, a clearly symmetric response is appeared in both lateral directions.

Figs. 14(a) and 14(b) explains the relation between the ratio V^* and the ratio Y^* in the lateral dimension of the hydrodynamic domains where the cylindrical pier center is the origin point. The ratio V^* is defined by

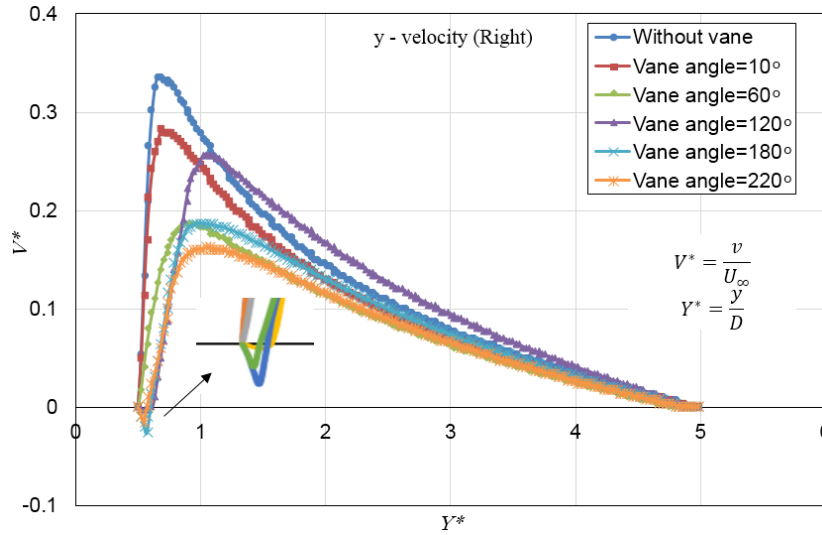
$$V^* = \frac{v}{U_{\infty}} \quad (11)$$

Where: v : is the flow in the y-axis direction (lateral direction of the domain).

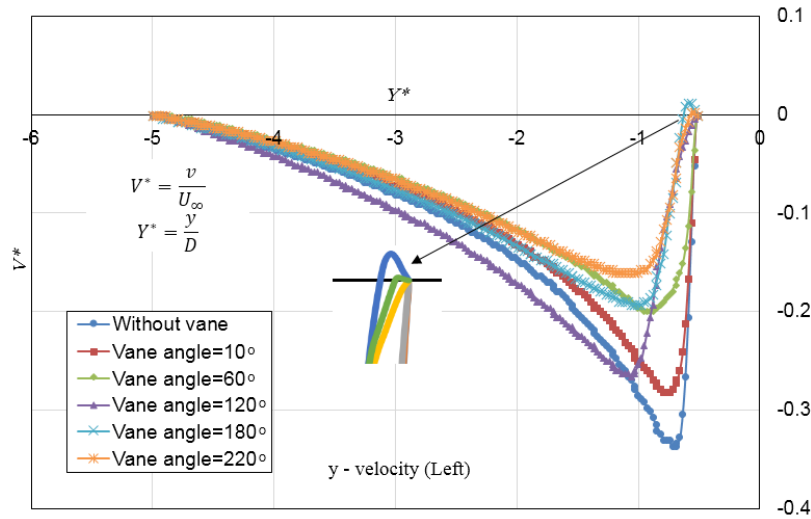
The figure is also sketched to reveal the mutation, which happens in the flow pattern between two different cases with and without the curved vane. It is obvious from the Figs. 14(a) and 14(b) that the ratio V^* at or near the surface of the cylindrical pier is equal to zero because of the no-slip boundary condition at the cylindrical pier. The ratio V^* increases gradually with an increase in the ratio Y^* , which is occurred due to the growth and evolution in the flow velocity. Beyond that, the ratio V^* decreases gradually with progress in the values of the ratio Y^* until it reaches zero owing to the assumed no-slip boundary condition imposed at the edges of the domain. Again, the figure reveals clearly symmetric response in both lateral directions.

Figs. 15(a) and 15(b) deals with the alteration between the ratio Y^* and the ratio U^* in the longitudinal dimension of the hydrodynamic domains where the cylindrical pier center is the origin point. The figure is sketched to reveal the mutation that happens in the flow pattern between two different cases; which are with and without the curved vane.

It is obvious from the Figs. 15(a) and 15(b) that the ratio U^* at or near the surface of the cylindrical pier is equal to zero because of the no-slip boundary condition at the cylindrical pier. The ratio U^* increases gradually until the ratio Y^* approximately become 4.5 or -4.5, this happens due to the growth and evolution in the flow velocity in the region confined between the side surface of the cylindrical pier and the edge of the boundary. After that, the ratio U^* decrease gradually until it reaches zero due to the no-slip boundary condition, which is imposed at the edges of the domain.



(a)



(b)

Fig. 14 (a) Variation of the ratio V^* with the ratio Y^* (right side) and (b) Variation of the ratio V^* with the ratio Y^* (left side)

Again, the figure reveals clearly symmetric response in both lateral directions. For interesting, the flow velocity magnitude represents the resultant of their components in x and y-directions.

6. Conclusions

The computational fluid dynamic analysis is employed to investigate the stream flow, which past a circular cylinder with curved vane of various angles have been performed at laminar flow regime.

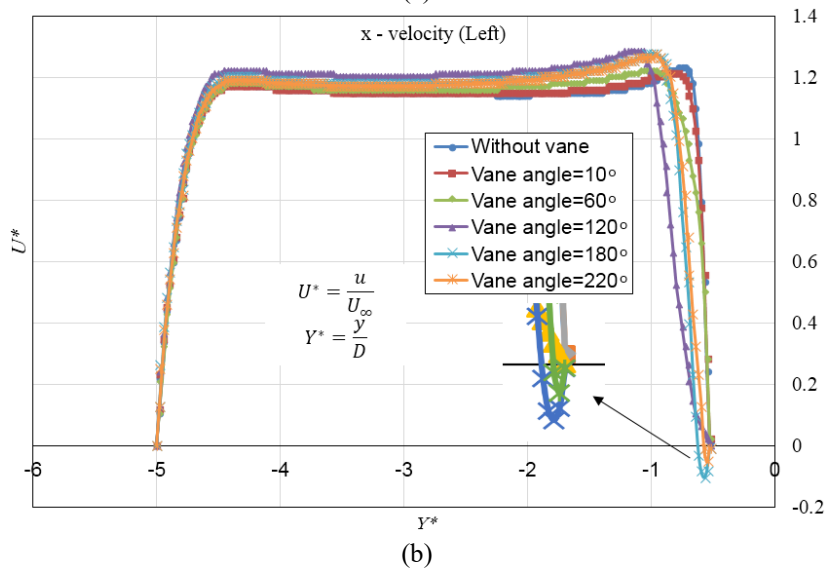
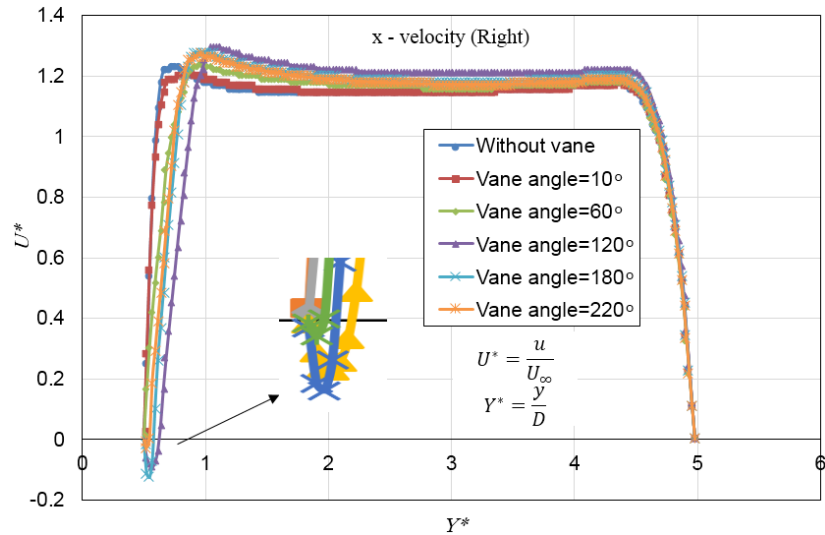


Fig. 15 (a) Variation of the ratio U^* with the ratio Y^* (right side) and (b) Variation of the ratio U^* with the ratio Y^* (left side)

The major objective of this numerical analysis is to investigate the influence of curved vane of various angles on the flow field around cylinder. The analysis has clearly shown that the curved vane structure is the responsible element for producing the bubbles between the rear edges of the curved vane and the upstream of the cylindrical pier, also the size of the bubbles which is produced in the wake region of the cylindrical pier is more influence by the curved vane angle. Here, we must mention that the angle (or the circumference) of the curved vane has a noticeable and major impact on the flow pattern which is surrounded the cylindrical pier. The structure of streamlines shows the deformation which is occurred in the fluid due to the presence of the curved vane, while the flow

velocity vector shows the change in the flow velocity direct due to the presence of the curved vane. Moreover, when the mobile flow separation point along the curved vane merge with the mobile flow separation point along the cylindrical pier, the upstream bubbles will be vanished this occur when the vane angle range between (190-220) degree. Here, along the curved vane circumference, two different processes will happen and these processes have essential role in produce and evolution of the bubbles these processes are flow separation and dissipation. From results, we can infer that the length and center of the downstream bubbles relies on the flow velocity alteration and the values of the curved vane angle. The relationship between downstream bubbles length and the curved vane angles will be more influenced by Reynolds number. The variation of the flow velocity along the radial line, which is started from the stagnation point at the upstream of the cylindrical pier toward any point in the fluid domain, shows the effect of the point location relatively to the location of the curved vane. There is not a mutation in flow velocity profile in lateral and longitudinal direction respectively.

References

- Abdulhussein, I.A., Qasim, R.M. and Al-Asadi, K. (2019), "Pier scouring reduction using a strip guide flow panel device", *RUDN J. Eng. Res.*, **20**(3), 229-235. <https://doi.org/10.22363/2312-8143-2019-20-3-229-235>.
- Ahmed, R.A. (2015), "Simulation of unsteady flow around a cylinder", *Wasit J. Eng. Sci.*, **3**(2), 28-49. <https://doi.org/10.31185/ejuow.vol3.iss2.38>.
- Alam, M.M., Sakamoto, H. and Moriya, M. (2003), "Reduction of fluid forces acting on a single circular cylinder and two circular cylinders by using tripping rods", *J. Fluid. Struct.*, **18**(3-4), 347-366. <https://doi.org/10.1016/j.jfluidstructs.2003.07.011>.
- Ali, M.S.M., Doolan, C.J. and Wheatley, V. (2011), "Low Reynolds number flow over a square cylinder with a splitter plate", *Phys. Fluids*, **23**(3), 033602. <https://doi.org/10.1063/1.3563619>.
- Becker, S., Lienhart, H. and Durst, F. (2002), "Flow around three-dimensional obstacles in boundary layers", *J. Wind Eng. Ind. Aerod.*, **90**(4-5), 265-279. [https://doi.org/10.1016/s0167-6105\(01\)00209-4](https://doi.org/10.1016/s0167-6105(01)00209-4).
- Bimbato, A.M., Alcântara Pereira, L.A. and Hirata, M.H. (2011), "Study of the vortex shedding flow around a body near a moving ground", *J. Wind Eng. Ind. Aerod.*, **99**(1), 7-17. <https://doi.org/10.1016/j.jweia.2010.10.003>.
- Bordbar, A., Sharifi, S. and Hemida, H. (2021), "Prediction of scour around single vertical piers with different cross-section shapes", *Ocean Syst. Eng.*, **11**(1), 43-58. <https://doi.org/10.12989/ose.2021.11.1.043>.
- Dahkil, S.F., Gabbar, T.A. and Jaber, D.K. (2014), "Numerical study of the initial pressure and diameters ratio effect on the jet ejector performance", *Basra J. Eng. Science*. **14**(1), 122-135.
- Deng, Y., Yang, J., Xiao, L. and Shen, Y. (2014), "Frequency analysis of wave run-up on vertical cylinder in transitional water depth", *Ocean Syst. Eng.*, **4**(3), 201-213. <https://doi.org/10.12989/ose.2014.4.3.201>.
- Graf, W.H. and Istiarto, I. (2002), "Flow pattern in the scour hole around a cylinder", *J. Hydraulic Res.*, **40**(1), 13-20. <https://doi.org/10.1080/00221680209499869>.
- Hsieh, T. and Chen, J. (2006), "Emergence of attached recirculating eddy for flow around a circular cylinder asymmetrically placed in a channel", *J. Mar. Sci. Technol.*, **14**(3), 147-154. <https://doi.org/10.51400/2709-6998.2068>.
- Hwang, J.Y. and Yang, K.S. (2007), "Drag reduction on a circular cylinder using dual detached splitter plates", *J. Wind Eng. Ind. Aerod.*, **95**(7), 551-564. <https://doi.org/10.1016/j.jweia.2006.11.003>.
- Kwon, K. and Choi, H. (1996), "Control of laminar vortex shedding behind a circular cylinder using splitter plates", *Phys. Fluids*, **8**(2), 479-486. <https://doi.org/10.1063/1.868801>.
- Qasim, R.M. and Jabbar, T.A. (2021), "An analytic study of the effect of a vane on the hydraulic field around a cylinder", *INCAS Bull*, **13**(3), 123-139. <https://doi.org/10.13111/2066-8201.2021.13.3.11>
- Osirin, M.F., Azmi, A.M., Yusoff, H. and Razak, N.A. (2019), "Effect of shroud hole on the force

- characteristics of a circular cylinder”, *Int. J. Eng. Adv. Technol.*, **9**(1), 5929-5935. <https://doi.org/10.35940/ijeat.a3030.109119>.
- Rajani, B.N., Kandasamy, A. and Majumdar, S. (2009), “Numerical simulation of laminar flow past a circular cylinder”, *Appl. Math. Model.*, **33**(3), 1228-1247. <https://doi.org/10.1016/j.apm.2008.01.017>.
- Ramli, N.A., Mohd Azmi, A., Abdul Hamid, A.H., Kamarul Baharin, Z.A. and Zhou, T. (2021), “Effect of cylinder gap ratio on the wake of a circular cylinder enclosed by various perforated shrouds”, *CFD Lett.*, **13**(4), 51-68. <https://doi.org/10.37934/cfdl.13.4.5168>.
- Saha, A.K., Muralidhar, K. and Biswas, G. (2003), “Investigation of two- and three-dimensional models of transitional flow past a square cylinder”, *J. Eng. Mech.*, **129**(11), 1320-1329. [https://doi.org/10.1061/\(asce\)0733-9399\(2003\)129:11\(1320\)](https://doi.org/10.1061/(asce)0733-9399(2003)129:11(1320)).
- Sharma, B. and Barman, R.N. (2020), “Steady laminar flow past a slotted circular cylinder”, *Phys. Fluids*, **32**(7), 073605. <https://doi.org/10.1063/5.0007958>.
- Wang, R., Xin, D. and Ou, J. (2020), “Three-dimensional characteristics and axial flow pattern in the wake flow of an oblique circular cylinder”, *J. Wind Eng. Ind. Aerod.*, **206**, 104381. <https://doi.org/10.1016/j.jweia.2020.104381>.
- Wu, J., Qiu, Y.L., Shu, C. and Zhao, N. (2014), “Flow control of a circular cylinder by using an attached flexible filament”, *Phys. Fluids*, **26**(10), 103601. <https://doi.org/10.1063/1.4896942>.
- Xu, Y., Fu, S., Chen, Y., Zhong, Q. and Fan, D. (2013), “Experimental investigation on vortex induced forces of oscillating cylinder at high Reynolds number”, *Ocean Syst. Eng.*, **3**(3), 167-180. <https://doi.org/10.12989/ose.2013.3.3.167>.
- Zhang, X.T., Li, Z.Y., Fu, S.X., Ong, M.C. and Chen, Y. (2014), “Study of the flow around a cylinder from the subcritical to supercritical regimes”, *Ocean Syst. Eng.*, **4**(3), 85-200. <https://doi.org/10.12989/ose.2014.4.3.185>.
- Zhu, H. and Zhou, T. (2019), “Flow around a circular cylinder attached with a pair of fin-shaped strips”, *Ocean Eng.*, **190**, 106484. <https://doi.org/10.1016/j.oceaneng.2019.106484>.